

Molecular-statics and molecular-dynamics study of diffusion along [001] tilt grain boundaries in Ag

Chun-Li Liu

Solid State Division, Oak Ridge National Laboratory, Oak Ridge, Tennessee 37830

S. J. Plimpton

Sandia National Laboratories, Albuquerque, New Mexico 87185

(Received 25 July 1994)

Self-diffusion parameters of Ag along $\Sigma 5(310)[001]$ and $\Sigma 13(320)[001]$ tilt grain boundaries are determined using both molecular-statics (MS) and molecular-dynamics (MD) techniques with a Ag potential based on the embedded-atom method. The MS calculations provide the diffusion energetics in the low-temperature regime for possible diffusion paths along the grain boundaries, while the MD simulations provide information on the effect of temperature on the diffusion parameters. The MD results indicate that diffusion mechanisms change from low temperatures to high temperatures. In the low-temperature regime, interstitial-related diffusion mechanisms are dominant. Vacancy-related diffusion mechanisms, while unimportant at low temperatures, become dominant at high temperatures due to increased vacancy concentration and mobility. These observations are supported by changing slopes in the Arrhenius plots for both our simulation results and experimental data. The calculated diffusion parameters are in satisfactory agreement with available experimental results.

I. INTRODUCTION

Mechanisms of grain boundary (GB) diffusion are of considerable interest¹⁻³ since diffusion in metals typically occurs more rapidly along GB's than through the lattice. Fast GB diffusion plays a significant role in a variety of metallurgical phenomena, such as microstructural stability, GB segregation, Coble creep, sintering, cellular precipitation, and intermixing in multiple-layer structures. It is generally believed that GB diffusion occurs through diffusion of point defects along the GB's. In particular, vacancy-related mechanisms are believed to be dominant in GB diffusion.^{2,3} However, recent experimental⁴ and theoretical modeling results⁵ for diffusion along [001] tilt boundaries indicate that, at low temperatures, interstitial-related diffusion mechanisms likely play a dominant role instead of vacancy-related mechanisms. The experimental results obtained by Ma and Balluffi⁴ at relatively low temperatures, when compared to values in the literature at high temperatures, also reveal that there are competing diffusion mechanisms at work at different temperatures, as evidenced by changing slopes in the Arrhenius plots of their diffusion data. This change in mechanism from low to high temperature has not been explained with direct experimental or theoretical evidence. Here we provide a simulation-based explanation.

In previous work,⁵ theoretical modeling of GB diffusion using molecular statics (MS) with embedded-atom method (EAM) potentials⁵ yielded consistent results with experiments in the low-temperature regime. This is primarily due to two factors. One is that the atomic energies computed from EAM potentials are highly sensitive to the atom's local environment. This makes EAM potentials particularly suitable for dealing with the inhomogeneity in structures such as grain boundaries. Another factor is that the calculations were per-

formed at the molecular-statics limit of 0 K. Therefore, the calculated diffusion parameters are only valid in a restricted range of low temperatures provided that the diffusion mechanisms do not change. High-temperature diffusion studies are needed to completely understand diffusion mechanisms along GB's as a function of temperature. Molecular dynamics (MD) is an alternative approach for obtaining such information.

In this paper, MS calculations were performed for two grain boundaries to investigate vacancy-related diffusion mechanisms as a function of temperature. MD simulations were carried out to extract diffusion parameters at higher temperatures up to the melting point, T_m . Combining the MS and MD results provides a more complete view of GB diffusion mechanisms and effects across a wide range of temperatures.

The organization of the paper is as follows. In Sec. II, the EAM potentials and computational methods are briefly described. MS results from previous work⁵ and the additional calculations performed for this paper are discussed in Sec. III. MD results are presented in Secs. IV and V. Finally, conclusions are drawn in Sec. VI.

II. THE EMBEDDED-ATOM METHOD AND COMPUTATIONAL TECHNIQUES

A. The embedded-atom method

The EAM was developed by Daw and Baskes⁶ as a semiempirical method for calculating the total energy of an arbitrary arrangement of atoms in a metal. In the EAM formalism the energy of an atom consists of two components: a sum of electrostatic pairwise interactions with each of its near neighbors, and an energy to embed the atom in the local-electron density created by its near neighbors. These components provide a "many-body"

effect sensitive to the atom's local environment, making possible the accurate treatment of low-symmetry systems such as free surfaces, interfaces, and grain boundaries.⁶ The free parameters in the EAM energy functions are determined empirically by fitting to several measured bulk properties, such as equilibrium lattice constants, sublimation energies, bulk moduli, elastic constants, vacancy formation energies, and heats of formation for dilute alloy solutions. The EAM functions developed by Adams, Foiles, and Wolfer (AFW) (Ref. 7) were used in the present study. These functions are nearly identical to the standard ones developed by Foiles, Baskes, and Daw,⁸ but they are fit to more accurate estimates of the vacancy formation energy.

B. Computational method

The grain boundaries for this study, symmetric $\Sigma 5(310)[001]$ and $\Sigma 13(320)[001]$ tilt boundaries, were created by joining unrelaxed and rotated bicrystals together. The tilt axis of the boundaries is along the z direction. Periodic boundary conditions were used in the GB plane directions (y and z), but not in the direction normal to the GB plane (x). This creates an infinite GB plane sandwiched between two free surfaces. The spacing between the GB plane and the free surfaces is large enough that the interaction between the GB and free surfaces is negligible. The total number of atoms in the simulation cell was about 2000. The GB was then relaxed at 0 K using molecular-statics (MS) techniques. The relaxed structure was used to perform both the MS and molecular-dynamics (MD) simulations. For the MD simulations performed at a given temperature, the simulation cell was first expanded uniformly in all three directions, using a linear thermal expansion coefficient for Ag calculated using the EAM.⁹

During MD simulations, the atoms near the free surfaces were constrained to move within their (310) or (320) planes (no motion perpendicular to the planes). This damps the motion of atoms near the free surfaces, but keeps the grain boundary centered in the simulation cell, enabling good statistics for diffusion parameters to be generated.¹⁰ By checking snapshots during the MD simulations we verified that in the temperature ranges simulated only those atoms near the grain boundary plane moved dramatically.

The MD simulations were performed at a constant volume, constant number of atoms, and constant energy, consistent with the microcanonical ensemble. Initial velocities of the atoms were assigned according to the Boltzmann distribution for a chosen MD simulation temperature. As the simulation progressed the forces acting on the atoms were calculated using the EAM potential for Ag,⁷ and the temperature of the ensemble was kept equilibrated near the chosen temperature by Langevin dynamical techniques. The simulations were run for 100–250 ps (20–50 000 time steps), and the trajectories of the atoms as a function of time were recorded. Atomic self-diffusion in the grain boundary within a width of $\delta = 10.0 \text{ \AA}$ (roughly two lattice plane spacings) was measured. This was done by computing the mean-squared

displacement of the individual atoms in each of three directions x , y , and z .

The collective mean-squared displacement (MSD) data as a function of time were used to calculate the diffusion coefficient D at a given temperature, which is given by classical diffusion theory as

$$D = \frac{\sum [(x_i - x_{i0})^2 + (y_i - y_{i0})^2 + (z_i - z_{i0})^2]}{6Nt}, \quad (1)$$

where x_i , y_i , and z_i are the coordinates of individual atoms at a given time, x_{i0} , y_{i0} , and z_{i0} are the initial coordinates of the atoms, N is the total number of atoms within the grain boundary, and t is the total MD simulation time. The sum is over all the atoms within the grain boundary width. Thus the slope of a MSD curve vs time is proportional to the diffusion coefficient.

The activation energy Q for grain boundary diffusion was obtained by running the MD simulations at different temperatures T and fitting the results to the Arrhenius relationship

$$D = D_0 \exp(-Q/kT), \quad (2)$$

where D_0 is a preexponential factor. Thus the slope of the data in an Arrhenius plot of D vs $1/T$ yields the activation energy Q and the intersection of the data with the vertical axis yields D_0 .⁵

III. MOLECULAR-STATICS CALCULATIONS

Some diffusion parameters for symmetric $\Sigma 5(310)[001]$ and $\Sigma 13(320)[001]$ boundaries (along with other boundaries) were calculated using previous work⁵ using the molecular-statics technique and an EAM potential for Ag. In order to present a clear and complete picture, additional MS calculations were carried out for vacancy-related diffusion processes. The results are given in Tables I and II for $\Sigma 5(310)[001]$ and $\Sigma 13(320)[001]$ tilt boundaries, respectively. Corresponding boundary unit cells are indicated in Figs. 1 and 2 in accordance

TABLE I. Formation E_f , migration E_m , and activation ($Q = E_f + E_m$) energies calculated by molecular-statics techniques for several point defects and diffusive jump paths in a $\Sigma 5(310)[001]$ symmetric tilt grain boundary. A primed site is two (001) planes away from an unprimed site in the z direction.

Site No.	E_f (eV)	Jump path	E_m (eV)	Q (eV)
1	0.65	1→4	0.33	0.98
		1→3	0.57	1.22
2	0.49	2→4	0.90	1.39
		2→2'	0.64	1.13
		2→2	0.24	0.73
		2→3	0.71	1.20
3	0.79			
4	0.78	4→4'	0.46	1.24
i	0.33	$i \rightarrow 2 \rightarrow i'$	0.23	0.56

TABLE II. Formation E_f , migration E_m , and activation ($Q = E_f + E_m$) energies calculated using molecular statics for several point defects and jump paths in a $\Sigma 13(320)[001]$ symmetric tilt grain boundary. A primed site is two (001) planes away from an unprimed site in the x direction.

Site No.	E_f (eV)	Jump path	E_m (eV)	Q (eV)
1	0.84			
2	0.24	$1 \rightarrow 1'$	0.38	1.22
		$2 \rightarrow 2'$	0.91	1.15
		$2 \rightarrow 2$	0.07	0.31
3	0.85			
4	0.24	$4 \rightarrow 4'$	0.86	1.10
i	0.15	$i \rightarrow 2 \rightarrow i'$	0.38	0.53

with the structural unit model.¹² The open and filled symbol represent atoms in adjacent (001) planes in the [001] direction, and numbers identify different unique atoms in the unit cell.¹²

Both defect formation and migration energies were calculated with MS techniques. A vacancy was created by removing an atom at the grain boundary. An interstitial site between the planes (the letter i) was identified by adding an atom in a relatively open region in the grain boundary and relaxing the entire structure. The difference in the total energy of the system before and after relaxation yields the defect formation energies. To calculate the migration energy of a defect, the defect was moved along a minimum-energy path toward a neighboring site in a series of small steps. At each step the position of the defect was held fixed and the entire system relaxed around it. This enabled the energy along the entire

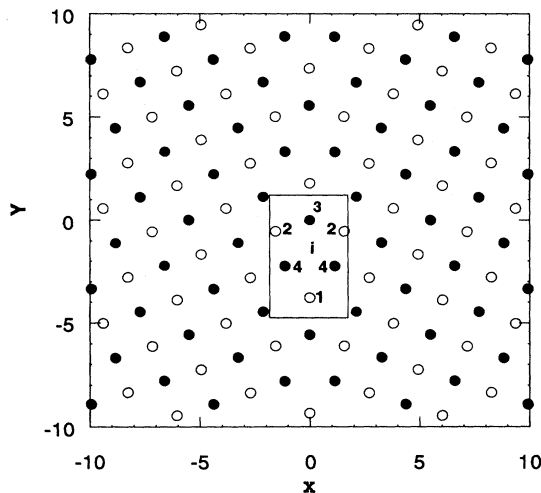


FIG. 1. Structure of the $\Sigma 5(310)[001]$ grain boundary after molecular-statics relaxation. A repeating boundary unit cell is indicated. Open and filled symbols represent adjacent stacking planes. Numbers identify unique atom positions in the unit cell; the letter i marks the position of an interstitial at the grain boundary.

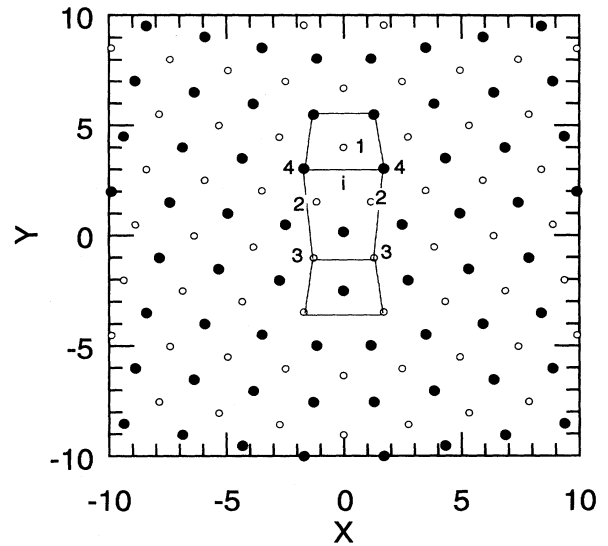


FIG. 2. Structure of the $\Sigma 13(320)[001]$ grain boundary obtained from molecular-statics relaxation. A boundary unit cell is outlined. Open and filled symbols represent two stacking planes. Numbers identify atom positions in the unit cell; the letter i marks the position of an interstitial at the grain boundary.

diffusion path to be calculated, and a saddle point along the path identified. The migration energy is then the difference in the system energy between the states, with defects at its initial equilibrium site and at the saddle point. In order to find the optimal diffusion path, various jump paths were attempted, and corresponding migration energies calculated. A primed jump site is two (001) planes away from an unprimed site in the z direction. The activation energies listed in the tables are the sum of defect formation and migration energies. All the data in Tables I and II are for vacancy jump paths except the last entries, which are for interstitials.

From the defect formation energy data, it is seen that the interstitial formation energies are the lowest. However, at site 2 of the $\Sigma 5(310)[001]$ boundary, and sites 2 and 4 of the $\Sigma 13(320)[001]$ boundary, vacancy formation energies are also comparably low. The low formation energies indicate that concentrations of these defects are relatively high at a given temperature.

As seen in Table I, for vacancy-related diffusion in the $\Sigma 5(310)[001]$ boundary, the lowest-energy path is $1 \rightarrow 4$ (0.98 eV). However, it does not contribute to diffusion, since the corresponding correlation coefficient is zero.⁵ The next-lowest-energy path is $2 \rightarrow 2'$ along the tilt axis (1.13 eV), followed by transverse jumps $2 \rightarrow 2$ (0.73 eV). Similar trends in the vacancy-related diffusion mechanisms also exist in the $\Sigma 13(320)[001]$ boundary. Vacancy jumps with low activation energies are all preferred along the tilt axis of grain boundaries. The activation energies of vacancy-related diffusion paths are almost a factor of 2 higher than that of interstitial-related diffusion paths. Many of the vacancy-related jumps have similar activation energies, indicating that several types of vacancy

jumps may occur simultaneously at a given temperature.

For interstitials, we found that interstitials moved via interstitialcy jumps, $i \rightarrow 2 \rightarrow i'$ in which the interstitial at site i pushed an atom at site 2 toward the site i' , and thus a concerted jump was performed. Formation and migration energies of an interstitial in both boundaries are both very low, resulting in much lower activation energies for the interstitialcy jumps. This is presumably due to the relatively open structures of these GB's. High concentrations of the interstitials due to low formation energies and high mobility due to low migration energies are the reason that interstitial-related diffusion mechanisms are dominant in these boundaries at low temperatures. The activation energies at low temperatures ($T < \frac{1}{3}T_m$) for Ag $\Sigma 5(310)[001]$ and $\Sigma 13(320)[001]$ tilt boundaries determined by Ma and Balluffi⁴ were about 0.70 eV, very close to the values calculated here for the interstitial-related diffusion mechanisms. On the other hand, although vacancy concentrations are comparable to interstitials, high migration energies prevent them from moving easily in the GB's at low temperatures.

IV. MD RESULTS AND DISCUSSION

The mean-squared displacement of atoms in the grain boundary region as a function of the MD simulation time at several temperatures is displayed in Fig. 3. The slopes of the curves are proportional to the diffusion coefficients through the relationship given in Eq. (1). The diffusion coefficients determined by fits to the mean-squared displacement vs time curves were then plotted against inverse temperature ($1/kT$, kT in eV), as shown in Figs. 4 and 5 for the $\Sigma 5(310)[001]$ and $\Sigma 13(320)[001]$ boundaries. The slopes of the curves are proportional to the activation energy Q for grain boundary diffusion within a temperature range. The intersections of the curves with

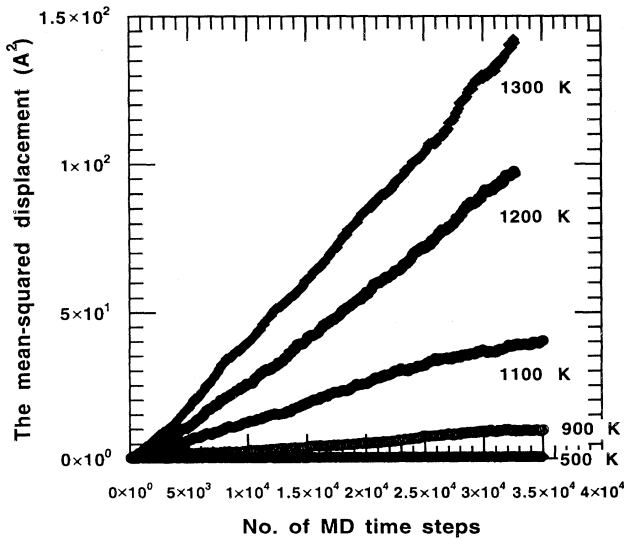


FIG. 3. The mean-squared displacement vs simulation time in the molecular-dynamics simulations of the $\Sigma 5(310)[001]$ grain boundary.

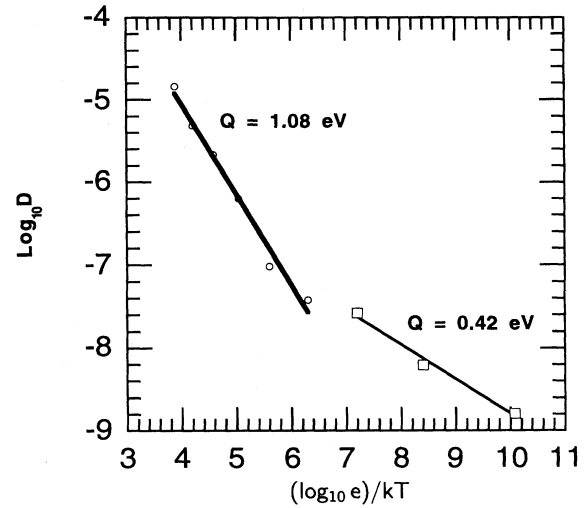


FIG. 4. The Arrhenius plot (kT in eV) for the $\Sigma 5(310)[001]$ grain boundary with activation energies Q determined by linear fitting to the data. Two regimes with different slopes are recognizable; the transition temperature is around 700 K.

the vertical axis give the values of D_0 . The values for these parameters determined by fitting to the data in the two figures are shown in Table III. We also directly compared our MD simulation results with experimental data from Ref. 4. This was done by multiplying both sides of Eq. (2) by the grain boundary width $\delta = 10.0 \text{ \AA}$, and then plotting the δD values against the normalized inverse temperature T_m/T , as shown in Fig. 6. The experimental data from Ref. 4 were obtained at the low-temperature regime, but extended here all the way to high-temperature regime in order to see the trend in Arrhenius plot. The data from literature indicated in Fig. 6 were ob-

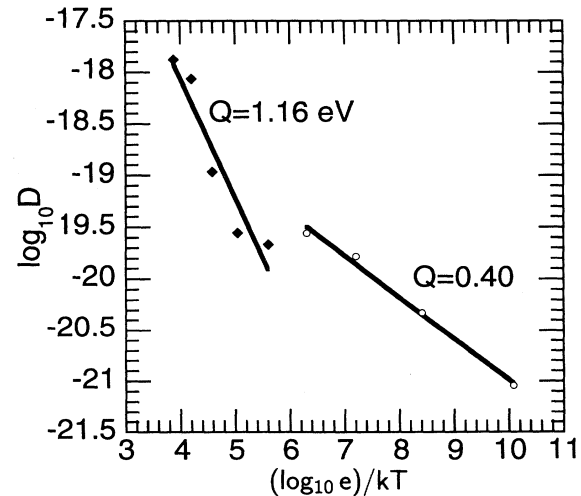


FIG. 5. The Arrhenius plot (kT in eV) for the $\Sigma 13(320)[001]$ grain boundary with activation energies Q . Again there are two regimes with different slopes; in this case the transition temperature is around 800 K.

TABLE III. Diffusion parameters determined from molecular-dynamics simulations of two tilt grain boundaries.

Boundary	D_0 (cm ² /s)	Q (eV)
$\Sigma 5(310)[001]$ (low T)	2.4×10^{-5}	0.42
$\Sigma 5(310)[001]$ (high T)	2.1×10^{-1}	1.08
$\Sigma 13(320)[001]$ (low T)	1.1×10^{-4}	0.40
$\Sigma 13(320)[001]$ (high T)	3.7×10^{-1}	1.16

tained at high temperatures, and were directly cited from Ref. 4. There is an obvious change in the slopes of Arrhenius plots around a temperature of ~ 600 K from the two sets of experimental data.

A distinct feature in the Arrhenius plots from MD simulations is also seen in Fig. 6, which shows that the simulated data fall into two different temperature regimes with different slopes: a low-temperature regime covering 500–700 and 500–800 K for $\Sigma 5(310)[001]$ and $\Sigma 13(320)[001]$, respectively, and a high-temperature regime from 800–1300 and 900–1300 K for $\Sigma 5(310)[001]$ and $\Sigma 13(320)[001]$, respectively. The activation energies obtained in the low-temperature regime are 0.42 and 0.40 eV, while in the high-temperature regime they are 1.08

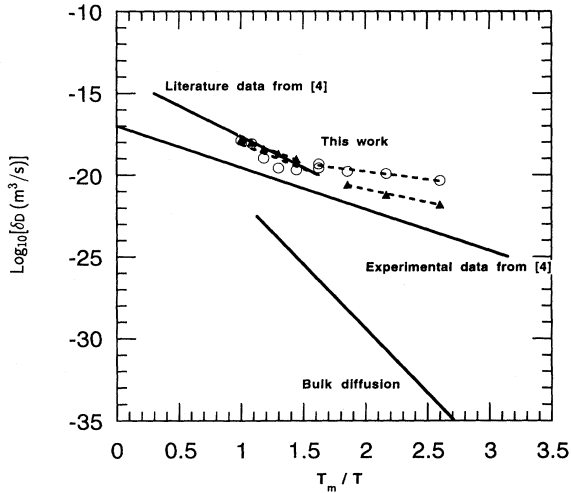


FIG. 6. Comparison of molecular-dynamics simulation results with available experimental data. The solid lines are data from Ref. 4. The circles and triangles are the $\Sigma 13(320)[001]$ and $\Sigma 5(310)[001]$ simulation data, obtained by multiplying Eq. (2) by the grain boundary width δ (delta in the figure), and plotting δD against the normalized temperature T_m/T (T_m is taken to be 1300 K for normalization in order to compare our simulation results with experimental results from Ref. 4). The dashed lines are fits to the simulation data. The upper curvature from experimental data (Ref. 4) at low temperatures (extended to high temperatures in the figure) to the literature data obtained at high temperatures can be seen near 2.0 of T_m/T . A similar trend was found from the simulation data.

and 1.16 eV for $\Sigma 5(310)[001]$ and $\Sigma 13(320)[001]$, respectively. A common feature for both boundaries is that the activation energies in the high-temperature regime are about a factor of 2 higher than those in the low-temperature regime. In agreement with the MS calculations, we found that activation energies from the MD simulations in the low-temperature regime are consistent with interstitial-dominated diffusion mechanisms, while the MD activation energies in the high-temperature regime are close to the values associated with vacancy-related diffusion mechanisms. This is evidence that the dominant diffusion mechanisms have changed from interstitial related to vacancy related. It is also interesting to note that the transition temperature for $\Sigma 5(310)[001]$ was around 700 K, and 800 K for the $\Sigma 13(320)[001]$ from the MD simulations, while experiments found a similar transition temperature at about 600 K, as shown in Fig. 6, where one can see that there is a transition from experimental data from Ref. 4 by Ma and Balluffi (lower solid line) to literature data (upper solid line) for grain boundary diffusion in Ag.

This transition can be understood if we consider the fact that the two important factors contributing to GB diffusion are the point defect concentrations and their mobility. In the low-temperature regime, only those defects with low formation and migration energies can dominate GB diffusion processes, such as those of interstitials. In the high-temperature regime, vacancy diffusion processes with effective high activation energies can be activated due to increased concentration and mobility. From our MS and MD simulation results, it is clear that vacancy-related GB diffusion mechanisms, while unimportant at low temperatures, become dominant at high temperatures. In this case, the fundamental jumps presented in Tables I and II are still important, although other types of jumps, such as multiple or coordinated jumps and direct interchange via the “ring” mechanism, may also become feasible.

Figure 6 shows that, in the high-temperature regime, the diffusion coefficients from the MD simulations are in good agreement with experimental results, while in the low-temperature regime they are higher than the values determined by Ma and Balluffi⁴ by 1–2 orders of magnitude. However, experimental measures of D typically have an uncertainty of at least 2–3 orders of magnitude.⁴ The MD activation energies (1.08–1.16 eV) in the high-temperature regime are also in good agreement with the experimental values.⁴ The activation energies calculated from MD simulations in the low-temperature regime are lower (0.40–0.42 eV) than the experimental values (about 0.70 eV).⁴

V. CONCLUSIONS

Based on the MS and MD simulation results presented for diffusion along [001] tilt grain boundaries, we draw the following conclusions.

(1) Interstitial-related diffusion mechanisms play a dominant role in GB diffusion at low temperatures due to much lower formation and migration energies. In contrast, the activation energies of vacancy-related diffusion

processes are much higher, indicating that they do not make significant contributions to low-temperature GB diffusion.

(2) Vacancy-related diffusion mechanisms, while unimportant at low temperatures, become dominant at high temperatures due to increased concentration and mobility of GB vacancies. Many vacancy-related diffusion processes with similar activation energies may occur simultaneously.

(3) The above conclusions are supported by both our MS and MD simulation results and experiments by Ma and Balluffi,⁴ in that two regions of distinct slope in the transition from low to high temperatures were observed in Arrhenius plots in both cases.

(4) The diffusion parameters determined from the MS and MD simulations were in satisfactory agreement with experiments.

ACKNOWLEDGMENTS

C.L.L. acknowledges that this research was sponsored in part by the Division of Materials Science, U.S. Department of Energy, under contract No. DE-AC05-84OR21400 with Martin Marietta Energy Systems, Inc. The work of S.J.P. was performed at Sandia National Laboratories, operated for the DOE under Contact No. DE-AC04-76DP00789. The MD computer simulations discussed here were performed on a nCUBE2 supercomputer at Sandia, with a version of the DYNAMO EAM code modified for parallel computation by S.J.P.¹³ The original DYNAMO code was written by Stephen Foiles and Murray Daw of Sandia, whom we thank for many useful discussions.

¹D. Turnbull and R. E. Hoffman, *Acta Metall.* **4**, 97 (1956).

²N. L. Peterson, *Int. Metall. Rev.* **28**, 65 (1983).

³R. W. Balluffi, *Metall. Trans.* **13B**, 527 (1982).

⁴Qing Ma and R. W. Balluffi, *Acta Metall. Mater.* **41**, 133 (1993).

⁵Qing Ma, C. L. Liu, J. B. Adams, and R. W. Balluffi, *Acta Metall. Mater.* **41**, 2143 (1993).

⁶M. S. Daw and M. I. Baskes, *Phys. Rev. Lett.* **50**, 1285 (1983).

⁷J. B. Adams, S. M. Foiles, and W. G. Wolfer, *J. Mater. Res.* **4**, 102 (1989).

⁸S. M. Foiles, M. I. Baskes, and M. S. Daw, *Phys. Rev. B* **33**,

7983 (1986).

⁹S. M. Foiles and M. S. Daw, *Phys. Rev. B* **38**, 12643 (1988).

¹⁰S. J. Plimpton and E. D. Wolf, *Phys. Rev. B* **41**, 2712 (1990).

¹¹M. S. Daw, S. M. Foiles, and M. I. Baskes, *Mater. Sci. Rep.* **9**, 251 (1993).

¹²R. W. Balluffi and A. Brokman, *Scr. Metall.* **17**, 1027 (1983).

¹³S. J. Plimpton and B. A. Hendrickson, in *Materials Theory and Modeling*, edited by J. Broughton, P. Bristowe, and J. Newman, MRS Symposia Proceedings No. 291 (Materials Research Society, Pittsburgh, 1992), p. 37.